OPEN ACCESS Freely available online

PLOS ONE

Dynamic Oxygen-Enhanced MRI of Cerebrospinal Fluid

Taha M. Mehemed[1], Yasutaka Fushimi[1]*, Tomohisa Okada[1], Akira Yamamoto[1], Mitsunori Kanagaki[1], Aki Kido[1], Koji Fujimoto[1], Naotaka Sakashita[2], Kaori Togashi[1]

1 Department of Diagnostic Imaging and Nuclear Medicine, Kyoto University Graduate School of Medicine, Kyoto, Japan, **2** Toshiba Medical Systems Corporation, MRI Systems Development Department Otawara-shi, Tochigi, Japan

Abstract

Oxygen causes an increase in the longitudinal relaxation rate of tissues through its T1-shortening effect owing to its paramagnetic properties. Due to such effects, MRI has been used to study oxygen-related signal intensity changes in various body parts including cerebrospinal fluid (CSF) space. Oxygen enhancement of CSF has been mainly studied using MRI sequences with relatively longer time resolution such as FLAIR, and T1 value calculation. In this study, fifteen healthy volunteers were scanned using fast advanced spin echo MRI sequence with and without inversion recovery pulse in order to dynamically track oxygen enhancement of CSF. We also focused on the differences of oxygen enhancement at sulcal and ventricular CSF. Our results revealed that CSF signal after administration of oxygen shows rapid signal increase in both sulcal CSF and ventricular CSF on both sequences, with statistically significant predominant increase in sulcal CSF compared with ventricular CSF. CSF is traditionally thought to mainly form from the choroid plexus in the ventricles and is absorbed at the arachnoid villi, however, it is also believed that cerebral arterioles contribute to the production and absorption of CSF, and controversy remains in terms of the precise mechanism. Our results demonstrated rapid oxygen enhancement in sulcal CSF, which may suggest inhaled oxygen may diffuse into sulcal CSF space rapidly probably due to the abundance of pial arterioles on the brain sulci.

Citation: Mehemed TM, Fushimi Y, Okada T, Yamamoto A, Kanagaki M, et al. (2014) Dynamic Oxygen-Enhanced MRI of Cerebrospinal Fluid. PLoS ONE 9(6): e100723. doi:10.1371/journal.pone.0100723

Editor: Friedemann Paul, Charité University Medicine Berlin, Germany

Received March 5, 2014; **Accepted** May 29, 2014; **Published** June 23, 2014

Funding: This work was supported by JSPS KAKENHI Grant Number 25461815 and a sponsored research program, "Researches for improvement of MR visualization (No. 150100700014)" provided to one of the authors, Professor Kaori Togashi, by Toshiba Medical Systems Corporation, Japan. The funders had no role in study design, data collection and analysis, decision to publish, or preparation of the manuscript.

Competing Interests: This study was partly supported by Toshiba Medical Systems Corporation, the employer of Naotaka Sakashita who has a joint patent application about this research with Toshiba Medical Systems Corporation. There are no further patents, products in development or marketed products to declare. This does not alter the authors' adherence to all the PLOS ONE policies on sharing data and materials, as detailed online in the guide for authors. The details of patent application is as follows: "MAGNETIC RESONANCE IMAGING APPARATUS AND IMAGE PROCESSING APPARATUS" "Japanese patent application No. 2013-170529."

* Email: yfushimi@kuhp.kyoto-u.ac.jp

Introduction

Oxygen causes an increase in the longitudinal relaxation rate of tissues through its T1-shortening effect owing to its paramagnetic properties, no T2-shortening effect of oxygen is seen [1,2]. Due to such effects, magnetic resonance imaging (MRI) has been used to study oxygen-related signal intensity (SI) changes in various body organs, such as the lungs [3], brain [4], spleen, myocardium, subcutaneous fat, kidneys, bone marrow, liver and arterial blood [2,5,6]. The paramagnetic effect of deoxyhemoglobin has frequently been used in the brain to visualize blood-oxygen-level-dependent (BOLD) contrast as functional MRI [7,8], and the paramagnetic effect of the oxygen molecule itself has also been used to quantify the oxygen content of cerebrospinal fluid (CSF), and to visualize oxygen enhancement (OE) of CSF on MRI [9,10]. Fluid attenuated inversion recovery (FLAIR) imaging has been mainly used to visualize OE of CSF, since oxygen administration causes signal hyperintensity in CSF of the subarachnoid space on FLAIR [11,12].

CSF acts as a physical cushion for the brain, and plays an important role in its biological waste disposal. This fluid is known to be produced from the choroid plexus in the ventricles, transfers to the cisterns and is eventually absorbed by the arachnoid villi, after exchanging contents with the interstitial fluid of the brain. CSF has been widely visualized using MRI techniques such as MR cisternography [13,14], phase-contrast MRI [15,16] and MRI with inversion pulse technique [17], which have provided clues to various pathological processes occurring in the brain. Changes in the oxygen content of CSF are reportedly associated with injury to brain tissue [18], but the resting state of oxygen content and dynamic changes in oxygen content after oxygen inhalation remain unclear. Knowledge of oxygen changes in CSF is also important from the perspective of partial volume effects during imaging analysis, since most cerebral cortices and vessels are surrounded by CSF.

OE on MR (OEMR) imaging of CSF has mostly been studied using FLAIR [1,11,19], T1 value calculation with inversion recovery (IR)-sequences [2,10], and dynamic tracking has been performed with relatively longer time resolution [10,11]. Shorter imaging time without IR will lead to better temporal resolution, but sequences without IR have not been utilized. Fast advanced spin echo (FASE) is a similar sequence with half-Fourier acquisition single-shot turbo spin-echo (HASTE), which has been previously used to calculate T1 values with IR (IR-HASTE) [2,20]. This study compared FASE to FASE with IR (IR-FASE) in terms of the ability to dynamically track OE of CSF. We also

compared OE of sulcal CSF (CSFs) with that of ventricular CSF (CSFv) in each image.

Materials and Methods

Subjects

The approval of the ethics committee of Kyoto University (approval number: C491) and written informed consent were obtained. Fifteen healthy volunteers (12 men, 3 women; mean age, 32±6 years) were recruited, and written informed consent was obtained from all volunteers prior to enrolment.

MRI parameters

IR-FASE and FASE images were acquired using a 3-T MRI scanner (Toshiba Medical Systems, Otawara, Japan) using a 13-channel head coil and the following parameters in a single-slice axial acquisition at the level of 15 mm superior to the anterior commissure – posterior commissure line. **IR-FASE:** repetition time (TR), 9575 ms; echo time (TE), 48 ms; inversion time (TI), 1915 ms; matrix, 192×192, 1.37×1.37 mm; slice thickness, 7 mm; field of view (FOV), 263×263 mm; flip angle, 90°; bandwidth, 977 Hz/pixel; Number of averaging is two with additional one TR for echo stabilization. **FASE:** TR, 4500 ms; TE, 48 ms; matrix, 192×192, 1.37×1.37 mm; slice thickness, 7 mm; FOV, 263×263 mm; flip angle, 90°; bandwidth, 977 Hz/pixel; Number of averaging is two with additional one TR for echo stabilization.

Dynamic OEMR

Using IR-FASE (28.8 s/image, 38 measurements) and FASE (13.5 s/image, 80 measurements) to track OE of CSF, images were divided into three phases: 1) pre-oxygen administration (Pre-O_2), where subjects breathed normal room air (21% O_2) for 5 min; 2) 100% oxygen administration, where subjects breathed 100% O_2 at a flow rate of 15 L/min for 5 min; and 3) post-oxygen administration (Post-O_2), where subjects breathed normal room air (21% O_2) for 8 min. Oxygen was delivered through a non-rebreather mask that was firmly attached to cover the mouth and nose of the subject.

Image analysis

Images from each subject were segmented into CSF and non-CSF components using a trainable segmentation plugin of Fiji [21]. The segmented image was further processed as follows: a CSFs mask image and a CSFv mask image were created. CSFs and CSFv masks were then applied to each image (38 images for IR-FASE, 80 images for FASE) and total SI values for each image were calculated (Fig. 1).

Normalization was achieved by setting the mean SI of all dynamic images of Pre-O_2, O_2 and Post-O_2 as 1000. Maximum SI (maxSI) of CSF was calculated for each subject from the start of O_2 inhalation. Slope of SI (SI_{slope}) was calculated using a differential function for SI curve and maximum SI_{slope} ($maxSI_{slope}$) of CSF was then calculated for each subject from the start of O_2 inhalation. Approximation methods were determined by selecting best R^2 value for each approximation: linear curve fitting regression analysis was performed for the Pre-O_2 and Post-O_2 phases and polynomial curve fitting regression analysis for O_2 phase. Mean SI with standard error of CSFs and CSFv signal values in both IR-FASE and FASE independently, and R^2 values were calculated for each phase.

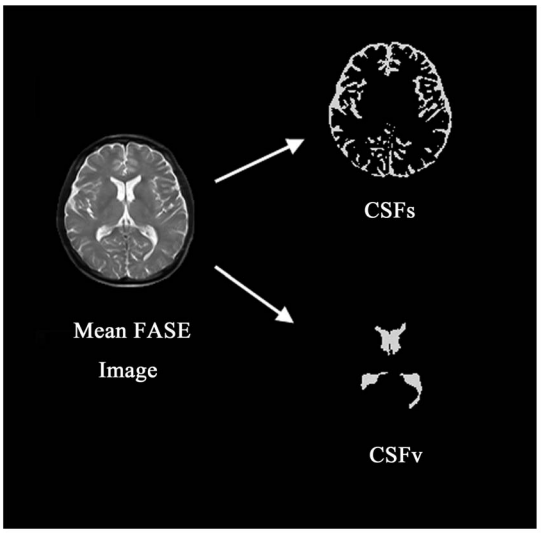

Figure 1. The mean image from FASE is segmented to create CSFs and CSFv masks, which are later applied to each image and total SI values for each image are calculated. The same process is performed for IR-FASE images. Note that the cavum velum interpositum was not included neirther to CSFv nor CSFs since it belongs to the cistern and it is not located at surfaces.
doi:10.1371/journal.pone.0100723.g001

Statistical analysis

Paired Student's t-test was conducted to compare maxSI and $maxSI_{slope}$ values for each volunteer in CSFs and CSFv between IR-FASE and FASE, with values of $p<0.05$ considered statistically significant. MedCalc version 12.2.1 software (MedCalc Software, Mariakerke, Belgium) was used.

Results

IR-FASE images

Pre-O_2 showed a linear correlation with time ($R^2 = 0.06$ for CSFs, and $R^2 = 0.61$ for CSFv). With oxygen administration, signal values of CSF increase in correlation with time, with a better polynomial curve fit for CSFs than for CSFv ($R^2 = 0.97$ for CSFs, and $R^2 = 0.76$ for CSFv). Post-O_2 signal values decrease with time, showing a linear curve fit ($R^2 = 0.68$ for CSFs, and $R^2 = 0.02$ for CSFv, respectively) (Fig. 2a, c).

FASE images

Pre-O_2 signals showed a linear correlation with time ($R^2 = 0.88$ for CSFs, and $R^2 = 0.77$ for CSFv). With oxygen administration, signal values of CSF rose in correlation with time, with a better polynomial curve fit in CSFs than CSFv ($R^2 = 0.94$ for CSFs, $R^2 = 0.72$ for CSFv). Post-O_2 signal values decrease with time, showing a linear curve fit ($R^2 = 0.94$ for CSFs, and $R^2 = 0.95$ for CSFv) (Fig. 2b, d).

Subtraction images

O_2 minus Pre-O_2 shows a positive SI difference, while Post-O_2 minus O_2 shows a negative SI difference in both IR-FASE and FASE images (Fig. 3).

IR-FASE vs. FASE

CSFs. Values of maxSI and $maxSI_{slope}$ were significantly higher for IR-FASE than for FASE ($p = 0.001$ and $p<0.0001$, respectively) (Table 1, Fig. 4a–b).

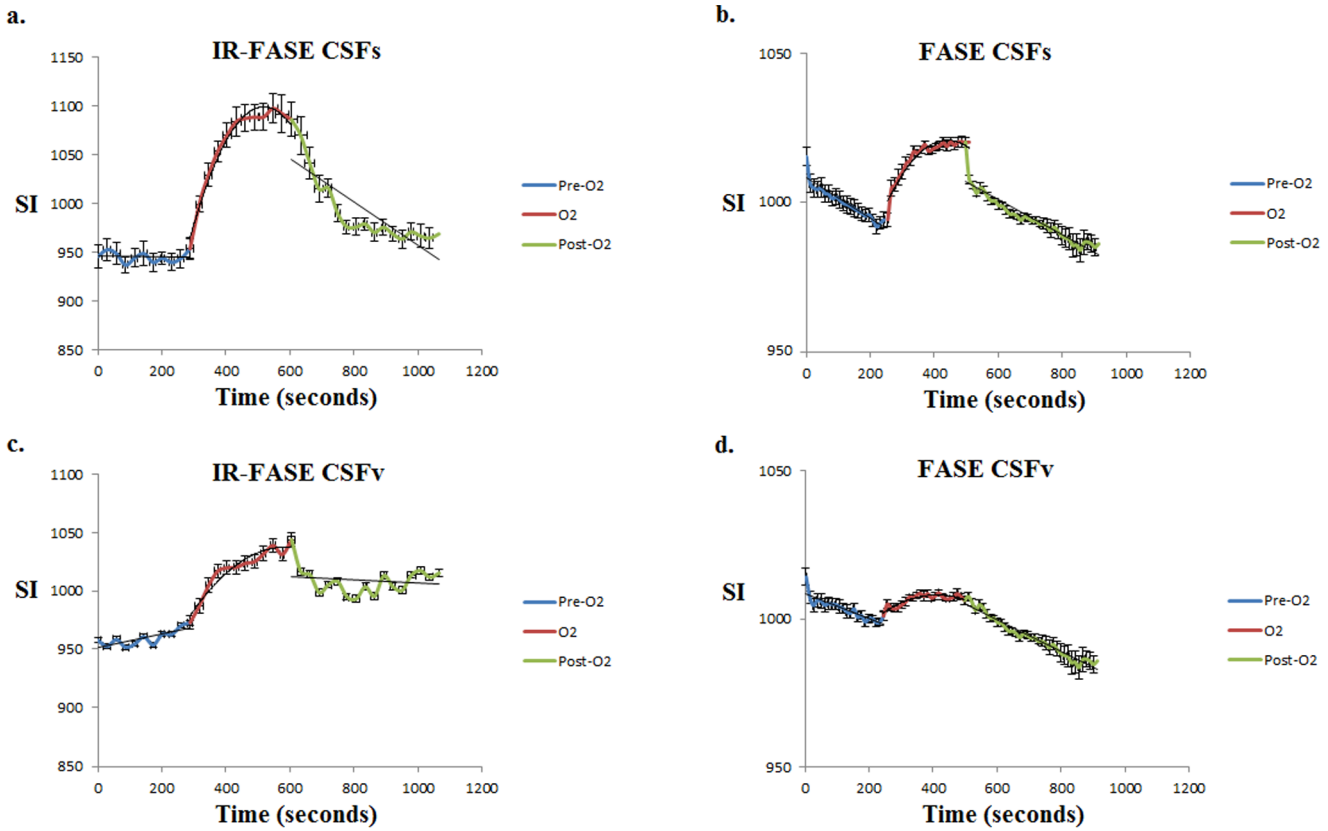

Figure 2. IR-FASE for Pre-O_2, Post-O_2 and O_2 phases of OE-MRI of CSFs (a) and CSFv (c), show higher SI with oxygen administration in CSFs compared to CSFv. FASE for Pre-O_2, Post-O_2 and O_2 phases of OE-MRI of CSFs (b) and CSFv (d), showing higher SI with oxygen administration in CSFs compared to CSFv. All data were shown with mean ± standard errors.
doi:10.1371/journal.pone.0100723.g002

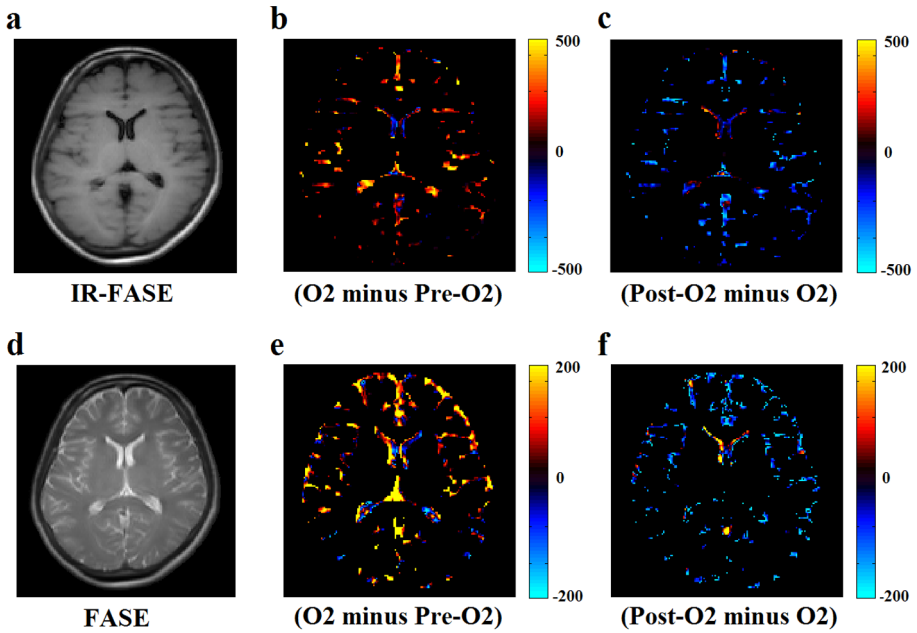

Figure 3. IR-FASE image (a), calculated IR-FASE images: "O_2 minus Pre-O_2" (b), "Post-O_2 minus O_2" (c). FASE image (d), calculated FASE images: "O_2 minus Pre-O_2" (e), "Post-O_2 minus O_2" (f). Calculated images of "O_2 minus Pre-O_2" show a positive SI difference (b, e), while calculated images of "Post-O_2 minus O_2" show a negative SI difference (c, f). Intra-ventricular high signals in "Post-O_2 minus O_2" images are assumed to come from the highly vascular choroid plexus.
doi:10.1371/journal.pone.0100723.g003

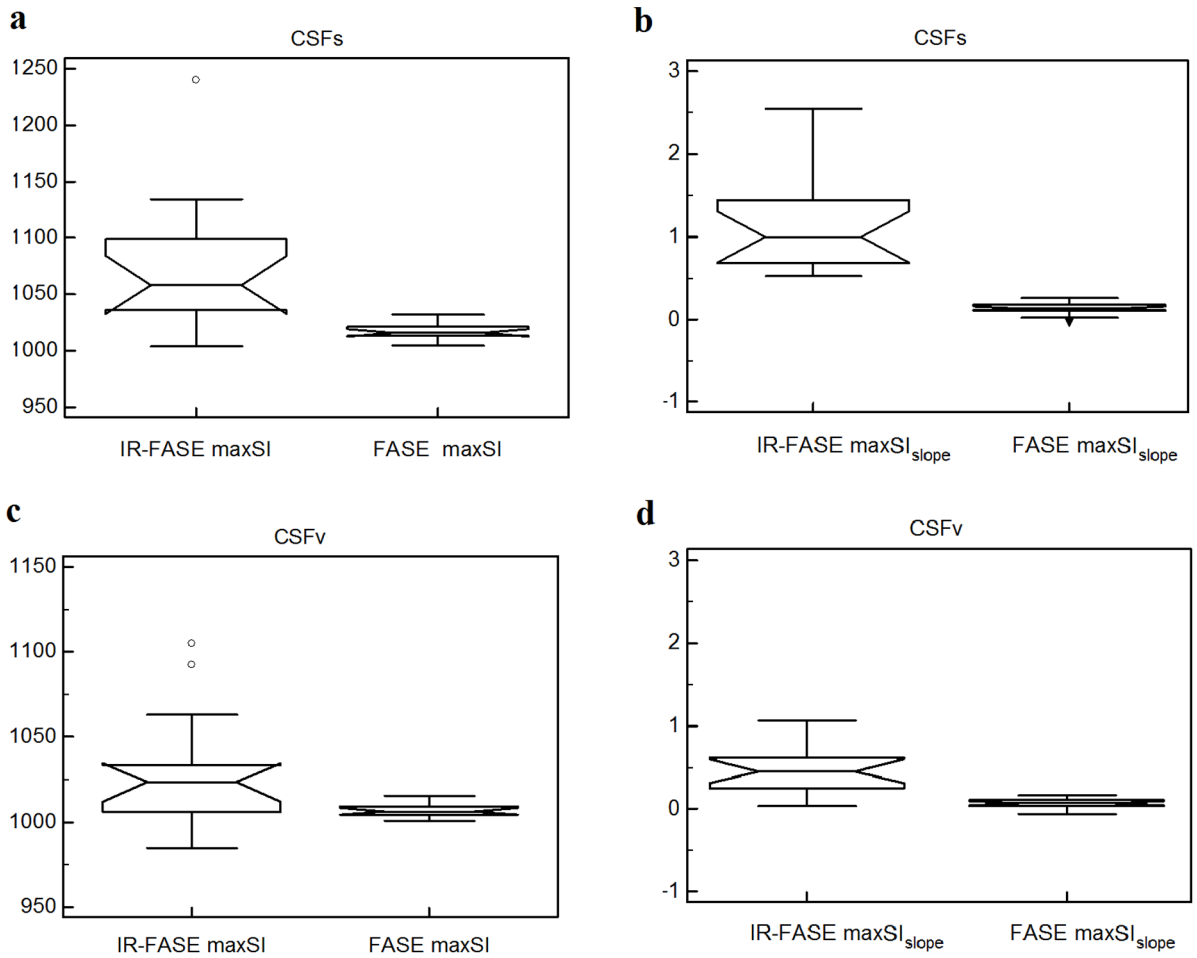

Figure 4. Box-and-whisker plots of IR-FASE vs. FASE maxSI and $maxSI_{slope}$ of CSFs (a–b) and CSFv (c–d). CSFs: maxSI and $maxSI_{slope}$ are significantly higher for IR-FASE than for FASE ($p = 0.001$ and $p < 0.0001$, respectively) (a, b). **CSFv**: maxSI and $maxSI_{slope}$ are significantly higher for IR-FASE than for FASE ($p = 0.034$, and $p = 0.0001$ respectively) (c, d).
doi:10.1371/journal.pone.0100723.g004

CSFv. Values of maxSI and $maxSI_{slope}$ were significantly higher for IR-FASE than for FASE ($p = 0.034$, and $p = 0.0001$, respectively) (Table 1, Fig. 4c–d).

CSFs vs. CSFv

CSFs showed significant higher maxSI and $maxSI_{slope}$ than CSFv in both IR-FASE ($p = 0.004$ and $p = 0.0003$ for maxSI and $maxSI_{slope}$, respectively) (Table 1, Fig. 5a–b) and FASE ($p < 0.0001$ and $p < 0.0001$ for maxSI and $maxSI_{slope}$, respectively) (Table 1, Fig. 5c–d).

Discussion

This study demonstrated dynamic tracking OE of CSF on both IR-FASE and FASE, since both methods showed positive signal increases during O_2 administration and maxSI data supported these findings. Rapid OE after O_2 administration displayed by SI_{slope} was also demonstrated and represented by $maxSI_{slope}$. In addition, OE of CSFs was visualized better than OE of CSFv on both IR-FASE and FASE. OE differences between CSFs and CSFv appeared largely compatible with previous studies of FLAIR with 5-min imaging sequence [1] and T1 value calculation with 7-

Table 1. MaxSI and $maxSI_{slope}$ for IR-FASE and FASE.

	maxSI			$maxSI_{slope}$		
	IR-FASE	**FASE**	**IR-FASE vs. FASE**	**IR-FASE**	**FASE**	**IR-FASE vs. FASE**
CSFs	1073.1±52.8	1015.9±8.3	P = 0.001*	1.277±0.639	0.197±0.078	P<0.0001*
CSFv	1028.1±34.3	1008.1±6.5	P = 0.034*	0.463±0.287	0.061±0.06	P = 0.0001*
CSFs vs. CSFv	P = 0.004*	P<0.0001*		P = 0.0003*	P<0.0001*	

All data were shown with mean ± standard errors. *Statistical significance (P<0.05).
doi:10.1371/journal.pone.0100723.t001

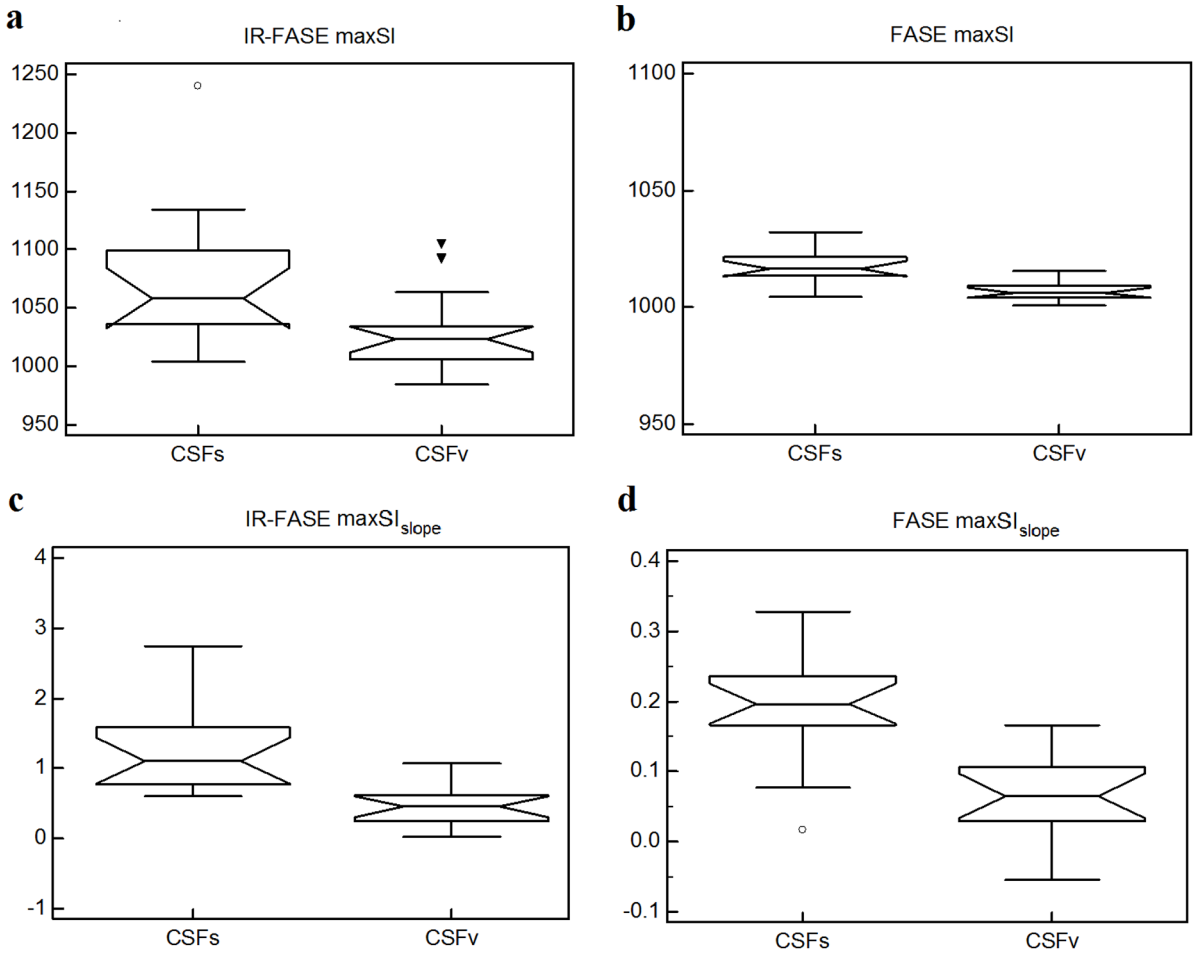

Figure 5. Box-and-whisker plots of CSFs vs. CSFv. Values of maxSI and $maxSI_{slope}$ are significantly higher for CSFs than for CSFv in both IR-FASE (maxSI, $p = 0.004$; $maxSI_{slope}$, $p = 0.0003$) (a, c) and in FASE (maxSI, $p < 0.0001$; $maxSI_{slope}$, $p < 0.0001$) (b, d).
doi:10.1371/journal.pone.0100723.g005

min imaging sequence [10], particularly in terms of the regional differences of T1 in CSF spaces such as basilar cisterns, lateral ventricles and cortical sulci. IR-FASE showed more OE of CSFs than FASE. Our results support previous reports of differences between OE of CSFs and OE of CSFv, but with higher temporal resolution than previously described [1,10].

CSF is traditionally thought to mainly form from the choroid plexus in the ventricles and is absorbed at the arachnoid villi [18,22]. While it is also believed that cerebral arterioles contribute to the production and absorption of CSF [23], controversy remains in terms of the precise mechanisms [24]. Capillaries in direct contact with the CSF form the blood-CSF barrier, where many constituents pass from the intra-arterial environment into CSF [25–27]. Since a linear relationship exists between arterial partial oxygen pressure (PaO_2) and CSF oxygen tension, increasing PaO_2 levels with 100% O_2 administration will lead to increased CSF levels of O_2. Oxygen diffuses into the CSF through the blood-CSF barrier, and this exchange occurs more in CSFs than in CSFv, due to the abundance of pial vessels on the surface of the brain compared to intra-ventricular vessels. The larger amount of intra-ventricular CSF might also cause more dilution of oxygen. Another cause might be the leaky areas of the blood-brain barrier near the pituitary gland, which would further facilitate oxygen diffusion into CSFs more than into CSFv. All of these mechanisms might contribute to the difference in OE between CSFs and CSFv [1]. A close relationship exists between CSF and arterial flows. Phase-contrast cine MRI has revealed the age-dependence of CSF flow increases and correlations with arterial flow [28]. Our results partly supported the idea that cerebral vessels are engaged in CSF production, since oxygen rapidly transfers to CSF from arteries.

IR sequences on MRI have been used to study OE of CSF in most previous reports [1,11,12]. Such OE was noticed on FLAIR images of anaesthetized patients and was initially explained by the effects of propofol, which has a similar T1 to CSF that would lead to incomplete nulling of the CSF signal [19]. However, later studies interpreted the hyperintensity as due to the paramagnetic effects of oxygen on CSF, in turn causing T1-shortening effects [11,12,29]. Arterial oxygen saturation by hemoglobin is close to 100% in healthy individuals. The partial pressure of dissolved oxygen in the blood represents a small fraction of the total oxygen concentration (less than 0.3%). The concentration of dissolved oxygen in the blood increased after oxygen inhalation and dissolved oxygen in the blood will diffuse into tissues according to the oxygen pressure gradient [1]. FLAIR is the sequence with an IR pulse to nullify the signal of CSF, so changes in T1 relaxation time of CSF interfere with suppression of the CSF signal. The T1-shortening effect has been utilized on FLAIR in various situations [30]. As HASTE sequence was used to calculate T1 values with IR [2], IR-FASE provides a similar T1-shortening

effect induced by oxygen as FLAIR, so FASE without IR might also show a weak T1-shortening effect. Since FASE shows T2 contrast, a T2-elongation effect cannot be excluded, although previous reports have claimed no apparent change in T2 relaxation time with oxygen administration [2]. The precise mechanisms remain unclear, and this appears to be the first study to dynamically track OE of CSF on FASE images.

OE-MRI might act as a non-invasive method for delineating pathological lesions occupying CSF spaces [31], and to better understand changes in oxygen status in the case of CSF-filled cystic tumors. OE-MRI might have the potential to non-invasively visualize cerebral collateral blood supply in cases of carotid occlusive disease through the diffusion of oxygen into CSF.

Several limitations exist, since these methods require a high degree of compliance from the imaged subject; firm fixation of the head was conducted in this study to reduce minor motions of the head. Second, quantification of OE such as T1 value calculation was not conducted in this study. We focused on higher temporal resolution of OE in this study, but rapid T1 calculation imaging is expected in the near future.

In conclusion, rapid oxygen enhancement of CSF can be dynamically tracked with both IR-FASE and FASE, and is observed more in CSFs than in CSFv, probably due to the abundance of pial arterioles on the brain surface compared to the intra-ventricular arterial system.

Acknowledgments

The authors are grateful to Kyoko Takakura for her technical support.

Author Contributions

Conceived and designed the experiments: YF TMM. Performed the experiments: YF AK KF. Analyzed the data: TO TMM AY. Contributed reagents/materials/analysis tools: MK TO NS. Wrote the paper: YF TMM KT.

References

1. Anzai Y, Ishikawa M, Shaw DW, Artru A, Yarnykh V, et al. (2004) Paramagnetic effect of supplemental oxygen on CSF hyperintensity on fluid-attenuated inversion recovery MR images. AJNR Am J Neuroradiol 25: 274–279.
2. Tadamura E, Hatabu H, Li W, Prasad PV, Edelman RR (1997) Effect of oxygen inhalation on relaxation times in various tissues. J Magn Reson Imaging 7: 220–225.
3. Stock KW, Chen Q, Morrin M, Hatabu H, Edelman RR (1999) Oxygen-enhanced magnetic resonance ventilation imaging of the human lung at 0.2 and 1.5 T. J Magn Reson Imaging 9: 838–841.
4. Losert C, Peller M, Schneider P, Reiser M (2002) Oxygen-enhanced MRI of the brain. Magn Reson Med 48: 271–277.
5. O'Connor JP, Jackson A, Buonaccorsi GA, Buckley DL, Roberts C, et al. (2007) Organ-specific effects of oxygen and carbogen gas inhalation on tissue longitudinal relaxation times. Magn Reson Med 58: 490–496.
6. Jones RA, Ries M, Moonen CT, Grenier N (2002) Imaging the changes in renal T1 induced by the inhalation of pure oxygen: a feasibility study. Magn Reson Med 47: 728–735.
7. Ogawa S, Lee TM, Kay AR, Tank DW (1990) Brain magnetic resonance imaging with contrast dependent on blood oxygenation. Proc Natl Acad Sci U S A 87: 9868–9872.
8. Okada T, Yamada H, Ito H, Yonekura Y, Sadato N (2005) Magnetic field strength increase yields significantly greater contrast-to-noise ratio increase: Measured using BOLD contrast in the primary visual area. Acad Radiol 12: 142–147.
9. Zaharchuk G, Busse RF, Rosenthal G, Manley GT, Glenn OA, et al. (2006) Noninvasive oxygen partial pressure measurement of human body fluids in vivo using magnetic resonance imaging. Acad Radiol 13: 1016–1024.
10. Zaharchuk G, Martin AJ, Rosenthal G, Manley GT, Dillon WP (2005) Measurement of cerebrospinal fluid oxygen partial pressure in humans using MRI. Magn Reson Med 54: 113–121.
11. Braga FT, da Rocha AJ, Hernandez Filho G, Arikawa RK, Ribeiro IM, et al. (2003) Relationship between the concentration of supplemental oxygen and signal intensity of CSF depicted by fluid-attenuated inversion recovery imaging. AJNR Am J Neuroradiol 24: 1863–1868.
12. Deliganis AV, Fisher DJ, Lam AM, Maravilla KR (2001) Cerebrospinal fluid signal intensity increase on FLAIR MR images in patients under general anesthesia: the role of supplemental O2. Radiology 218: 152–156.
13. Fushimi Y, Miki Y, Ueba T, Kanagaki M, Takahashi T, et al. (2003) Liliequist membrane: three-dimensional constructive interference in steady state MR imaging. Radiology 229: 360–365; discussion 365.
14. Yoshino N, Akimoto H, Yamada I, Nagaoka T, Tetsumura A, et al. (2003) Trigeminal neuralgia: evaluation of neuralgic manifestation and site of neurovascular compression with 3D CISS MR imaging and MR angiography. Radiology 228: 539–545.
15. Bhadelia RA, Bogdan AR, Wolpert SM, Lev S, Appignani BA, et al. (1995) Cerebrospinal fluid flow waveforms: analysis in patients with Chiari I malformation by means of gated phase-contrast MR imaging velocity measurements. Radiology 196: 195–202.
16. Bargallo N, Olondo L, Garcia AI, Capurro S, Caral L, et al. (2005) Functional analysis of third ventriculostomy patency by quantification of CSF stroke volume by using cine phase-contrast MR imaging. AJNR Am J Neuroradiol 26: 2514–2521.
17. Yamada S, Miyazaki M, Kanazawa H, Higashi M, Morohoshi Y, et al. (2008) Visualization of cerebrospinal fluid movement with spin labeling at MR imaging: preliminary results in normal and pathophysiologic conditions. Radiology 249: 644–652.
18. Oreskovic D, Klarica M (2010) The formation of cerebrospinal fluid: nearly a hundred years of interpretations and misinterpretations. Brain Res Rev 64: 241–262.
19. Filippi CG, Ulug AM, Lin D, Heier LA, Zimmerman RD (2001) Hyperintense signal abnormality in subarachnoid spaces and basal cisterns on MR images of children anesthetized with propofol: new fluid-attenuated inversion recovery finding. AJNR Am J Neuroradiol 22: 394–399.
20. Yang D, Kodama T, Tamura S, Watanabe K (1999) Evaluation of the inner ear by 3D fast asymmetric spin echo (FASE) MR imaging: phantom and volunteer studies. Magn Reson Imaging 17: 171–182.
21. Schindelin J, Arganda-Carreras I, Frise E, Kaynig V, Longair M, et al. (2012) Fiji: an open-source platform for biological-image analysis. Nat Methods 9: 676–682.
22. Alksne JF, Lovings ET (1972) Functional ultrastructure of the arachnoid villus. Arch Neurol 27: 371–377.
23. Greitz D (2004) Radiological assessment of hydrocephalus: new theories and implications for therapy. Neurosurg Rev 27: 145–165; discussion 166–147.
24. Cohen B, Voorhees A, Vedel S, Wei T (2009) Development of a theoretical framework for analyzing cerebrospinal fluid dynamics. Cerebrospinal Fluid Res 6: 12.
25. Bulat M, Klarica M (2011) Recent insights into a new hydrodynamics of the cerebrospinal fluid. Brain Res Rev 65: 99–112.
26. Moody DM (2006) The blood-brain barrier and blood-cerebral spinal fluid barrier. Semin Cardiothorac Vasc Anesth 10: 128–131.
27. Igarashi H, Tsujita M, Kwee IL, Nakada T (2014) Water influx into cerebrospinal fluid is primarily controlled by aquaporin-4, not by aquaporin-1: 17O JJVCPE MRI study in knockout mice. Neuroreport 25: 39–43.
28. Schmid Daners M, Knobloch V, Soellinger M, Boesiger P, Seifert B, et al. (2012) Age-specific characteristics and coupling of cerebral arterial inflow and cerebrospinal fluid dynamics. PLoS One 7: e37502.
29. Frigon C, Shaw DW, Heckbert SR, Weinberger E, Jardine DS (2004) Supplemental oxygen causes increased signal intensity in subarachnoid cerebrospinal fluid on brain FLAIR MR images obtained in children during general anesthesia. Radiology 233: 51–55.
30. Taoka T, Yuh WT, White ML, Quets JP, Maley JE, et al. (2001) Sulcal hyperintensity on fluid-attenuated inversion recovery mr images in patients without apparent cerebrospinal fluid abnormality. AJR Am J Roentgenol 176: 519–524.
31. Braga F, Rocha AJ, Gomes HR, Filho GH, Silva CJ, et al. (2004) Noninvasive MR cisternography with fluid-attenuated inversion recovery and 100% supplemental O(2) in the evaluation of neurocysticercosis. AJNR Am J Neuroradiol 25: 295–297.